



Swansea University
Prifysgol Abertawe



Cronfa - Swansea University Open Access Repository

This is an author produced version of a paper published in:

Biosensors and Bioelectronics

Cronfa URL for this paper:

<http://cronfa.swan.ac.uk/Record/cronfa50808>

Paper:

Teixeira, S., Abreu, C., Parkes, L., Davies, J., Yao, S., Sawhney, M., Margarit, L., Gonzalez, D., Pinto, I., et. al. (2019). Direct monitoring of breast and endometrial cancer cell epigenetic response to DNA methyltransferase and histone deacetylase inhibitors.. *Biosensors and Bioelectronics*, 111386
<http://dx.doi.org/10.1016/j.bios.2019.111386>

Released under the terms of a Creative Commons Attribution Non-Commercial No Derivatives License (CC-BY-NC-ND).

This item is brought to you by Swansea University. Any person downloading material is agreeing to abide by the terms of the repository licence. Copies of full text items may be used or reproduced in any format or medium, without prior permission for personal research or study, educational or non-commercial purposes only. The copyright for any work remains with the original author unless otherwise specified. The full-text must not be sold in any format or medium without the formal permission of the copyright holder.

Permission for multiple reproductions should be obtained from the original author.

Authors are personally responsible for adhering to copyright and publisher restrictions when uploading content to the repository.

<http://www.swansea.ac.uk/library/researchsupport/ris-support/>

Accepted Manuscript

Direct monitoring of breast and endometrial cancer cell epigenetic response to DNA methyltransferase and histone deacetylase inhibitors.

S.R. Teixeira, C.M. Abreu, L. Parkes, J. Davies, S. Yao, M.A. Sawhney, L. Margarit, D. Gonzalez, I. Mendes Pinto, L.W. Francis, R.S. Conlan



PII: S0956-5663(19)30465-8

DOI: <https://doi.org/10.1016/j.bios.2019.111386>

Article Number: 111386

Reference: BIOS 111386

To appear in: *Biosensors and Bioelectronics*

Received Date: 11 April 2019

Revised Date: 23 May 2019

Accepted Date: 30 May 2019

Please cite this article as: Teixeira, S.R., Abreu, C.M., Parkes, L., Davies, J., Yao, S., Sawhney, M.A., Margarit, L., Gonzalez, D., Pinto, I.M., Francis, L.W., Conlan, R.S., Direct monitoring of breast and endometrial cancer cell epigenetic response to DNA methyltransferase and histone deacetylase inhibitors., *Biosensors and Bioelectronics* (2019), doi: <https://doi.org/10.1016/j.bios.2019.111386>.

This is a PDF file of an unedited manuscript that has been accepted for publication. As a service to our customers we are providing this early version of the manuscript. The manuscript will undergo copyediting, typesetting, and review of the resulting proof before it is published in its final form. Please note that during the production process errors may be discovered which could affect the content, and all legal disclaimers that apply to the journal pertain.

2
3 **Direct monitoring of breast and endometrial cancer cell epigenetic response to DNA**
4 **methyltransferase and histone deacetylase inhibitors.**

5
6
7 **Authors**

8
9 S. R. Teixeira^{2,3}, C. M. Abreu⁴, L. Parkes^{1,3}, J. Davies^{1,3}, S. Yao^{1,3}, M. A. Sawhney^{1,3}, L. Margarit^{1,5}, D.
10 Gonzalez^{1,3}, I. Mendes Pinto⁴, L. W. Francis^{1,3}, R. S. Conlan^{1,3,*}

11
12 **Affiliations**

13 ¹Swansea University Medical School, Singleton Park, Swansea, SA2 8PP, UK

14 ²College of Engineering, Swansea University, Bay Campus, Swansea, SA1 8QQ, UK

15 ³Centre for NanoHealth, Swansea University, Singleton Park, Swansea, SA2 8PP, UK

16 ⁴International Iberian Nanotechnology Laboratory (INL), Portugal

17 ⁵Abertawe Bro Morgannwg University Health Board, Princess of Wales Hospital Bridgend, UK.

18 * corresponding author, r.s.conlan@swansea.ac.uk

19
20 **Keywords**

21 epigenetics; EIS; DNA methylation; histone acetylation; cancer cell lines
22
23
24
25
26
27
28
29
30
31
32
33

38 function and tumorigenesis. Therapeutic strategies based on DNA methyltransferase (DNMT) and histone
39 deacetylase (HDAC) inhibitors are currently in use and under development for the treatment of cancers.
40 Genome-wide DNA methylation profiling has been proposed for use in disease diagnosis, and histone
41 modification profiling for disease stratification will follow suit. However, whether epigenome sequencing
42 technologies will be feasible for rapid clinic diagnosis and patient treatment monitoring remains to be seen,
43 and alternative detection technologies will almost certainly be needed. Here we used electrochemical
44 impedance spectroscopy (EIS) employing a graphene-based screen-printed electrode system to directly
45 measure global DNA methylation and histone H3 acetylation to compare non-cancer and breast cancer cell
46 lines. We demonstrated that whilst global methylation was not useful as a differential marker in the
47 cellular systems tested, histone H3 acetylation was effective at higher chromatin levels. Using breast and
48 endometrial cancer cell models, EIS was then used to monitor cellular responses to the DNMT and HDAC
49 inhibitors 5-Aza-2'-deoxycytidine and suberoylanilide hydroxamic acid *in vitro*, and proved very effective
50 at detecting global cellular responses to either treatment, indicating that this approach could be useful in
51 following treatment response to epigenetic drugs. Moreover, this work reports the first combined analysis
52 of two epigenetic markers using a unified graphene-based biosensor platform, demonstrating the potential
53 for multiplex analysis of both methylation and acetylation on the same sample.

54 55 **1. Introduction**

56
57 Cancer cells undergo epigenetic changes in 5-methylcytosine distribution that include global DNA
58 hypomethylation and the hypermethylation of promoter CpG islands associated with tumor-suppressor
59 genes. DNA methylation is just one facet in the coordinated regulation of chromatin structure that also
60 involves discrete modifications to histone proteins, including histone H3 and H4 deacetylation, among
61 others, which collectively result in transcriptionally altered states (Capp, 2017; Jones and Baylin, 2007; Lo
62 and Zhou, 2018; Sheahan and Ellis, 2018).

63
64 Large-scale epigenomic studies have been made possible using established complex technologies. These
65 allow the genome-wide mapping of epigenetic marks, including DNA methylation and histone
66 modifications, which are critical for regulating gene expression. In turn, we are learning how mapping
67 aberrant alterations to these epigenetic marks can be used in clinical diagnostics (Bock et al., 2016; Butler
68 and Dent, 2013; Libertini et al., 2016; Rendeiro et al., 2016).

69
70 DNA methylation and histone modification biomarkers have several advantages that qualify them for
71 broad use as *in vitro* diagnostics and to support clinical decisions: (i) They can be cell-type-specific, yet
72 robust toward transient perturbations. (ii) They are binary marks (i.e., for a single cell and allele, an
73 epigenetic mark is either modified or not), which facilitates reliable measurements on heterogeneous
74 samples. (iv) The use of epigenetic markers to detect cancer sensitively is based on the premise that tumor-
75 derived chromatin/DNA is released into bodily fluids, or other remote samples, and can be detected by
76 abnormal DNA methylation and histone modification patterns (Bormann et al., 2018; Coleman and De,
77 2018; Graff-Baker et al., 2018; Singh et al., 2018; Xi et al., 2018; Zhang et al., 2018).

78
79 Current approaches to assess the epigenetic state currently target individual genetic loci to determine
80 histone modification (predominantly acetylation and methylation) and DNA methylation status. Bisulphite
81 sequencing has been the mainstay of DNA methylation analysis with methylated and hydroxymethylated
82 DNA immunoprecipitation (MeDIP and (h)MeDIP) methods coming online, whilst chromatin
83 immunoprecipitation (ChIP) is the research tool of choice for determining histone modifications. However,

87 include serum proteomics using mass spectrometry that whilst progressing in clinical feasibility studies,
88 require expensive and highly technical hardware, and expert users for sample and data analysis.

89
90 Electrochemical immunosensors using advances in nanomaterials are being developed for biosensing
91 applications (Zhu et al., 2015). For the detection of epigenetic modifications electrochemical analytical
92 methods offer several advantages over other techniques, such as surface plasmon resonance and atomic
93 force spectroscopy, in terms of sensitivity, simplicity and portability (Stewart and Tsui, 2018).
94 Furthermore, they offer limits of detection of methylated DNA within the levels reported to be found
95 circulating in plasma (Stewart and Tsui, 2018). In addition, instrumentation required to make such
96 measurements is low-cost, with instrument refinement reducing costs even further (Sawhney and Conlan,
97 2019). Gold and carbon -based electrode systems remain the most utilized working electrode materials,
98 despite many other materials having been evaluated (Krejцова et al., 2017), and have been used in screen
99 printed formats that offer low cost per unit, and do not require extensive preparation to obtain a pristine
100 surface prior to use. Graphene as a working electrode offers a high signal to noise ratio, and is easily
101 functionalized with antibodies when coated with polyaniline, which also serves a conductive polymer and
102 is used as an additive transducer layer to avoid the introduction of graphene surface defects (Gazze et al.,
103 2018; Teixeira et al., 2014a). Graphene offers a further advantage over gold electrodes for the detection
104 and quantification of DNA as it lacks the inherent absorption properties for unmodified DNA that are
105 displayed by gold surfaces due to affinity interactions (Koo et al., 2015). Here, we demonstrate the use of
106 a graphene-based immunosensor, where anti-5-methylcytosine (anti-5mc) and anti-acetylated histone H3
107 (anti-acH3) antibodies were directly coupled to a polyaniline-modified screen-printed graphene electrode
108 to detect DNA and chromatin using label-free EIS measurements. Using this system global levels of
109 methylated DNA and histone H3 acetylated chromatin levels were assessed in normal (MCF12A) and
110 cancer (MCF7) breast cell models, and MCF7 and HEC50 cells treated with a DNMT or HDAC inhibitors
111 were found to show alterations in DNA methylation or histone H3 acetylation respectively. Overall, this
112 study highlights the effectiveness EIS graphene immune sensors for the direct label- and amplification-free
113 detection of global epigenetic modifications in cancer cells, and thus their potential for monitoring
114 therapeutic efficacy.

115 116 **2. Materials and Methods**

117
118 **Cell culture and treatments.** MCF7 cells (ATCC, Maryland USA) were cultured in Eagle's Minimum
119 Essential Medium (Gibco, ThermoFisher Scientific, UK) supplemented with 10% (v/v) foetal bovine
120 serum (Gibco) and 0.01mg/ml insulin (Sigma-Aldrich, Missouri, USA). Hec50 cells (ATCC, Maryland
121 USA) were cultured in Dulbecco's Modified Eagle Medium: Nutrient Mixture F-12 (DMEM/F12) (Gibco,
122 ThermoFisher Scientific, UK) supplemented with 10% (v/v) fetal bovine serum (Gibco), 1% (v/v)
123 penicillin and streptomycin (Gibco), sodium bicarbonate and sodium pyruvate. MCF12A cells (ATCC,
124 Maryland USA) were cultured in Dulbecco's Modified Eagle Medium: Nutrient Mixture F-12
125 (DMEM/F12) (Gibco, ThermoFisher Scientific, UK) supplemented with 5% (v/v) horse serum (Gibco),
126 20ng/ml human epidermal growth factor, 100 ng/ml cholera toxin, 0.01 mg/ml bovine insulin and 500
127 ng/ml hydrocortisone 95%. All cell lines were grown at 37°C in a humidified atmosphere with 5% CO₂ to
128 90% confluency in T75 flasks (Corning, New York, USA) before collection. Cells were grown to 40% or
129 60% confluency respectively before exchanging full growth media for stripped media prior to treatment
130 with the DNMT inhibitor 5-Aza-2'-deoxycytidine (1 µM), suberoylanilide hydroxamic acid (2.5 µM) or
131 vehicle (DMSO).

Immunosensor assembly. Graphene-SPEs were purchased from DropSens (DRP-110GPH Metrohm UK Ltd, Runcorn, UK) and were composed of a carbon counter electrode, a silver pseudo-reference electrode, and a printed graphene working electrode (4 mm \varnothing). Electrical characterization of SPEs was performed by connecting the SPEs to the potentiostat/galvanostat *via* a suitable switch box (DropSens, Metrohm UK Ltd, Runcorn, UK). In order to mediate selective immunodetection of chromatin and gDNA to the graphene sensor surface, PANI functionalization was utilized, as previously described (Teixeira et al., 2014b).

Electrochemical measurements. CV and EIS were performed using a Metrohm Autolab PGSTAT302N equipped with FRA32M and DRP-DSC connector; control and analysis were provided through Nova software version 2.0.1 and higher (Metrohm UK Ltd, Runcorn, UK). CV procedures spanned -0.7 to 0.7 Volts starting and ending at 0V with a scan rate of 0.05 Volts per second. EIS procedures applied 50 frequencies between 1000 and 0.01 hertz, logarithmically distributed at an amplitude of 0.01 V_{RMS} on a DC bias of 0.1V with the reference electrode. EIS data was fitted to a R(C[R(RC)]) equivalent circuit model using a maximum of 300 iterations with weight factor applied.

Chromatin/gDNA detection and quantification. The functionalized biosensing platforms are based on impedance measurements resulting in changes of resistivity (Rct) following the binding of a chromatin or gDNA to the specific antibody immobilized on the sensor surface. Increasing concentrations of chromatin ranging from 0.0086 to 134 ng/ μ L for MCF12A, 0.0078 to 123 ng/ μ L for MCF7 and 0.0053 to 416 ng/ μ L for Hec50; and gDNA solutions, ranging from 0.0048 to 75 ng/ μ l for all cell lines, were prepared by dilution of 1708 ng/ μ L of chromatin and 75 ng/ μ L of gDNA stock solutions in media.

Chromatin immunoprecipitation. ChIP assays were performed using the Chromatrap® ChIP-seq kit following the manufacturers' instructions (Porvair Sciences Ltd, Wrexham, UK). Chromatin was quantified by Nanodrop 2000 (ThermoFisher Scientific) and visualized using agarose gel electrophoresis to ensure correct distribution of fragment sizes prior to immunoprecipitation. 1 μ g of each chromatin sample was used per ChIP with 2 μ g of relevant antibody; anti acetyl H3 antibody (Millipore, Darmstadt, Germany) or non-specific rabbit IgG (Chromatrap, Porvair Sciences Ltd, Wrexham, UK). qPCR was carried on the target gene *p21 forward primer* 5'-CCCACAGCAGAGGAGAAAGAA; *reverse primer* 5'-CTGGAAATCTCTGCCAGACA.

Methylated DNA immunoprecipitation. MeDIP assays were carried out using the Chromatrap MeDIP kit according to the manufacturers' protocol (Porvair Sciences Ltd, Wrexham, UK). gDNA was quantified by Nanodrop 2000 (ThermoFisher Scientific) and visualized using agarose gel electrophoresis to ensure correct distribution of fragment sizes prior to immunoprecipitation. 500 ng DNA was used per MeDIP with 1 μ g kit supplied anti-5-methylcytosine antibody or non-specific mouse IgG and linker. Samples were neutralized, and amplification of enriched methylated DNA carried out at the *CXCL12 locus forward primer* 5'-CTCATTTCAGTTCCCGCCATC; *reverse primer* 5'-GCCGCTTATTGTCCCTGTG.

Western blotting. Total protein was extracted using RIPA buffer and quantified using the DC Protein assay (BioRad, Watford, UK). Relevant protein concentrations were separated by SDS PAGE. Proteins were transferred to PVDF membrane, blocked and probed with a 1/15,000 dilution of anti-acetyl H3 antibody (Millipore, Watford, UK) followed by ECL anti-rabbit IgG horse radish peroxidase (GE

179 **Dot blotting:** gDNA extracted and sheared as described for the MEDIP protocol was used for dot blotting.
180 Immun-Blot PVDF Membrane (BioRad, Watford, UK) was activated with methanol and equilibrated with
181 transfer buffer prior to spotting the membrane with 100ng heat denatured gDNA. A 1/300 dilution of the
182 primary antibody anti-5mC (Chromatrap Porvair Sciences Ltd, Wrexham, UK) was used to probe the
183 methylated DNA and detected with ECL anti-rabbit IgG horse radish peroxidase (GE Healthcare, Bucks,
184 UK).

185 3. Results

186 *Immunosensor assembly and functionalization*

187
188
189 Electrochemical impedance spectroscopy (EIS) is a label and amplification free technique that enables
190 direct molecular measurements on modified surface electrodes (Sánchez et al., 2008). Here, we adapted
191 our previously reported screen-printed electrode (SPE)-graphene/polyaniline (PANI) platform to detect
192 methylated DNA and acetylated histone H3 using anti-5mc and anti-acH3 antibodies respectively. Sensor
193 optimization using control DNA and chromatin extracted from cell line models established sensitivity
194 according to our established protocols (Teixeira et al., 2016).
195

196 Sensor assembly was evaluated using scanning electron microscopy and atomic force microscopy (Fig.
197 S1), and electron transfer properties determined against a redox probe and evaluated by cyclic
198 voltammetry (CV) and EIS. Unmodified graphene-SPEs showed a quasi-reversible electrochemical
199 response for the $[\text{Fe}(\text{CN})_6]^{3-/4-}$ redox couple with ΔE_p of 0.158 V and ΔI_p of 0.285 mA, respectively. After
200 10 cycles, the modification of graphene-SPE surface with PANI resulted in a ΔI_p increase of 0.894 mA
201 and a ΔE_p decrease of 2.898 V (Fig. 1A) attributed to positively charged amino groups of the PANI
202 molecule attracting the negative charge of $[\text{Fe}(\text{CN})_6]^{3-/4-}$ promoting electron transfer on the electrode
203 surface (Zor et al., 2013). A cyclic voltammogram of the SPE-graphene/PANI/Antibody electrode showed
204 a decrease peak-to-peak potential separation (ΔE_p of 0.547 V). Further, addition of the BSA blocking
205 agent to the SPE-graphene/PANI/Ab electrode surface gave rise to a change on the electrochemical
206 behavior of $[\text{Fe}(\text{CN})_6]^{3-/4-}$, leading to a ΔE_p increase of 0.258 V and decreased ΔI_p value of 0.546 mA.
207 BSA molecules cause masking of the electrode surface oxidation/reduction of the redox probe $[\text{Fe}(\text{CN})_6]^{3-}$
208 $/4-$ (Daniels and Pourmand, 2007).
209

210 EIS data are presented as Nyquist plots where the R_{ct} at the electrode surface is given by the semicircle
211 diameter obtained in EIS and can be used to define the interface properties of the electrode. The
212 unmodified graphene surface display fast electron-transfer properties ($R_{ct} = 884 \Omega$, Fig. 1B), which
213 increases following PANI deposition ($R_{ct} = 1.13 \text{ K}\Omega$, Fig. 1B). Following covalent attachment of anti-
214 acH3 antibody, the R_{ct} increased to 1.82 $\text{K}\Omega$ (Fig. 1B), demonstrating that electron exchange between the
215 redox probe and the electrode was impeded, and this was enhanced further when BSA was added to the
216 SPE-graphene/PANI/Ab ($R_{ct} = 2.09 \text{ K}\Omega$, Fig. 1B). Similar data was obtained for the anti-5mc antibody
217 sensor platform build (Fig. 1C and D). To define linear ranges for 5mc and acH3 concentrations, R_{ct}
218 values of genomic DNA (gDNA; 4.8pg/ μL - 75ng/ μL) and chromatin (8.6pg/ μL - 134ng/ μL) were
219 determined (Fig. 2A and B respectively).
220

221 *DNA methylation and histone H3 acetylation status in normal and breast cancer cell models*

220 $\Omega \pm 205 \Omega$, 75 ng/ μ L input gDNA) (Fig. 3A), consistent with global methylated DNA assessment made
221 using dot blotting (Fig. 3B). Single locus analysis of a CpG island in the 5'UTR of CXCL12, which
222 encodes the stromal cell derived factor 1 α protein commonly overexpressed in many cancers (Guo et al.,
223 2016), also demonstrated that DNA methylation levels were similar in both normal and cancer breast cell
224 types (Fig. 3C).

231
232 EIS also enabled direct measurement of global histone H3 acetylation (acH3) in MCF7 cells for e.g.,
233 4460 $\Omega \pm 50 \Omega$, 134 ng/ μ L input chromatin which was significantly higher than the levels measured in
234 MCF12A (3287 $\Omega \pm 589 \Omega$, 75 ng/ μ L input chromatin) (Fig. 3D), and this difference was confirmed by
235 protein blotting (Fig. 3E). Conversely ChIP analysis at the cyclin dependent kinase inhibitor 1 (p21) locus
236 revealed an 8-fold lower level in acetylation in MCF7 compared to MCF12A cells (Fig. 3F),
237 demonstrating that whilst globally the MCF7 genome is hyperacetylated compared to MCF12A cells, there
238 are also locus specific and therefore functional differences between these breast cancer cell types.
239 Suppression of p21 expression through loss of acetylation results in loss of cell cycle arrest, driving
240 proliferation, a hallmark of cancer cells, and is therefore expected in the cancer cell line.

241
242 EIS sensor measurements show that global measurement of epigenetic marks can be useful in
243 differentiating cancer and non-cancer cell types, and that combining epigenetic signatures may be
244 beneficial. For example, MCF7 (low methylation + high acetylation) can be distinguished from MCF12A
245 (low methylation + low acetylation). With the addition of other epigenetic marks an algorithm could be
246 developed to provide a cell specific signature.

247 248 ***Monitoring global response to decitabine and vorinostat treatments in cancer cell lines.***

249
250 Small chemical modifications that trigger chromatin remodeling through processes including DNA
251 methylation and histone acetylation are of increasing interest as therapeutic targets in cancer diseases due
252 to reversible nature of these epigenetic modifications (Dawson and Kouzarides, 2012; Flavahan et al.,
253 2017). For example, 5-Aza-2'-deoxycytidine (decitabine) is a strong inducer of DNA de-methylation and is
254 approved for the treatment of myelodysplastic syndrome (Mossman et al., 2010; Ramos et al., 2015), and
255 suberoylanilide hydroxamic acid (vorinostat) is a histone deacetylase inhibitor (HDACi) approved for the
256 treatment of cutaneous T cell lymphoma (Qu et al., 2017). The rapid detection of global epigenetic status
257 could represent a useful tool for risk assessment, diagnosis, and for treatment monitoring, complementing locus
258 specific analysis of tumor suppressor and oncogene epigenetic status in patients.

259
260 EIS was used to assess MCF7 and HEC50 cells for response to decitabine and vorinostat treatments (Fig. 4A
261 and D; Fig. 5A and D). The response of MCF7 cells to decitabine was readily distinguished using EIS
262 sensors at higher concentrations of input gDNA (≥ 15 ng/ μ L). For example, a $\Delta\Omega$ between untreated
263 (2630 $\Omega \pm 160 \Omega$ at 75 ng/ μ L) compared to treated (2130 $\Omega \pm 122 \Omega$ at 75ng/ μ L) was -500 Ω showing an
264 expected decrease in DNA following treatment. For endometrial cancer cells a similar trend was observed,
265 for example a mean $\Delta\Omega$ of -780 at 75ng/ μ L (Fig. 5A).

266
267 These responses were validated using a methylated DNA specific dot blot, where 100ng total gDNA
268 extracted from both MCF7 and HEC50 cells showed decreased intensity following treatment (Fig. 4B and
269 5B), and by MeDIP where the CpG island region of the CXCL12 gene was significantly demethylated. A

Acetylated histone H3 was similarly analyzed following exposure of cells to vorinostat. Significantly increased acetylation was observed in the treated samples compared to untreated controls in both MCF7 and HEC50 with $\Delta\Omega$ much greater compared to that observed for decitabine treatment (Fig. 4D and 5D). For MCF7, a $\Delta\Omega$ of +653 ($8173 \Omega \pm 99 \Omega$ treated, $7520 \Omega \pm 331 \Omega$ untreated) was measured in MCF7 at the highest input chromatin concentration of 24.6 ng/ μ L for untreated and 44 ng/ μ L for vorinostat treated, indicative of an increase in open chromatin architecture. For Hec50, a $\Delta\Omega$ of +4600 was ($7830 \Omega \pm 90 \Omega$ treated, $3230\Omega \pm 38 \Omega$ untreated) was obtained for 83.2 ng/ μ L for untreated cells and 58 ng/ μ L for treated cells).

Immunosensor performance was also validated by western blotting (Fig. 4E and 5E), and p21 ChIP where a 2.11 and 3.28 -fold increase in H3 acetylation following vorinostat treatment were measured in MCF7 and HEC50 respectively (Fig. 4F and 5F).

The use of EIS in monitoring cellular responses to drug treatment is clearly very effective, and such a monitoring would be of value in determining patient responses to such treatments, particularly if measurements could be made directly from free circulating methylated DNA and modified chromatin that are known to alter in patients.

4. Discussion

The adaptation of a graphene based EIS immunosensor has enabled for the first-time direct amplification-free and label-free detection of both DNA- and nucleosome- linked epigenetic modifications. The method developed here utilizes antibodies that have been validated and widely used for locus specific genome wide analysis associated with CHIP- and MeDIP- techniques, making comparison between EIS and epigenomic analysis more robust. The EIS method presents a snapshot of 'gross' epigenetic status rather than the 'statically global view' obtained from the assimilation of multi-loci epigenome datasets. The speed of signal acquisition compared to PCR or DNA sequencing is substantially improved as there is no requirement for template amplification. Furthermore, the relative simplicity of the analytical process and very low sample volumes lend this approach to clinical utility. This technology is envisioned to become a price competitive point-of-care system, where single use functional screen-printed electrodes are preferable to reusable systems due to the need to minimize false positive results that would likely occur due to incomplete biological sample removal from the biosensor surface. Future miniaturization of this technology, as printing techniques become more refined and with higher resolution, will go some way to reducing the associated waste stream. Current legislation necessitates that clinical samples are correctly handled of therefore sensor chips exposed to clinical material must be disposed of appropriately.

Cytosine methylation and gross histone H3 acetylation are regulatory mechanisms for, and established markers of, transcription repression and activation respectively. DNA methylation directs gene silencing through the establishment of condensed heterochromatic structures, whereas histone H3 acetylation results in the loss of association between lysine residues in histone tails and the negatively charged phosphate backbone of DNA resulting in transition to a euchromatic state. Furthermore, both mechanisms are the target of currently available therapeutics including decitabine, a cytosine analogue that functions as a DNA methylase transferase (DNMT) inhibitor. Following its incorporation into DNA during replication, decitabine irreversibly binds to DNMT1, sequestering it the site of interaction and rendering it ineffective.

321 Here we have reported differences between EIS measurements as a $\Delta\Omega$ value, as the exact amount of DNA
322 or chromatin present has not been directly determined. However, as total global DNA methylation levels
323 are estimated to be 0.7 – 2.8 mole percent i.e., moles of 5-methyl cytosine per 100 bases of total DNA in
324 eukaryotes (Hall, 1971), we estimate for example that 0.52-2.1ng/ μ L methylated DNA per 75ng/ μ L input
325 DNA is being detected in the EIS assay. Similarly, it is estimated that only 1.2% of chromatin is acetylated
326 at histone H3 (Roh et al., 2005), therefore we are detecting approximately 1.6 ng/ μ L acetylated histone H3
327 per 134ng/ μ L input chromatin.

328
329 DNA methylation levels were similar for normal and breast cancer cell lines tested using EIS suggesting
330 that global methylation without any selection of genetic loci is not useful in differentiating between the cell
331 types used in this study. In contrast, the level of global acetylation in the MCF7 cancer cell line was higher
332 than in the non-cancer MCF12A cells illustrating that, even in the absence of any pharmacological
333 treatment that can modify cellular epigenetic status, differences can be determined between cell types that
334 originate from the same tissue.

335
336 Using EIS sensors we were able to trace cellular response to treatments with DNMT or HDAC inhibitors,
337 monitoring the respective decreases in DNA methylation or increases in histone H3 acetylation. The
338 response of both breast and endometrial cancer cells to decitabine and vorinostat was as expected with
339 differentiation between cell responses to either treatment detectable at detectable very low levels of input
340 DNA or chromatin. With this detection platform available it will now be possible to monitor patient
341 responses to treatment directly from patient samples.

342
343 With the recent surge in global efforts to map epigenomes across cancer types and patient cohorts (Bock et
344 al., 2016; Libertini et al., 2016; Rendeiro et al., 2016; Xi et al., 2018) it is becoming possible to associate
345 global epigenetic changes with disease status using statistical approaches. We propose that multiplex EIS
346 could be used to simultaneously assess several epigenetics marks, and that such an approach could
347 accurately diagnose and even stage disease progression directly from patient samples. Such an approach
348 would obviate the need for DNA sequencing or indeed the complex and ongoing processes of identifying
349 and characterizing circulating protein biomarkers. The use of a multi-epigenetic marker algorithm coupled
350 with the $\Delta\Omega$ differential quantification against known and predetermined/preprogrammed standards
351 provides an obvious and compelling strategy that now needs to be exploited.

352 353 354 **5. Conclusions**

355
356 Whilst a number of DNA methylation sensors have been reported (Krejcová et al., 2017) no single
357 platform has yet emerged as a preferred solution for accurate and rapid methylation testing. The use of
358 biosensors in monitoring changes in global methylation levels in response to cancer cell treatment with
359 decitabine is reported here for the first time. The development of biosensors for detection of histone
360 acetylation lags significantly behind that of DNA methylation biosensors, and has to date been limited to
361 fluorescent based approaches (Wang et al., 2017). The system presented in the current study uses an
362 antibody-based approach, and employs the same platform used for DNA methylation detection. Using this
363 system, we were able to demonstrate for the first-time the amplification and label free immuno-detection
364 of histone H3 acetylation, and monitor responses of breast and endometrial cancer models to vorinostat, a
365 drug that has undergone clinical trials for the treatment of advanced breast cancer (Luu et al., 2018). The

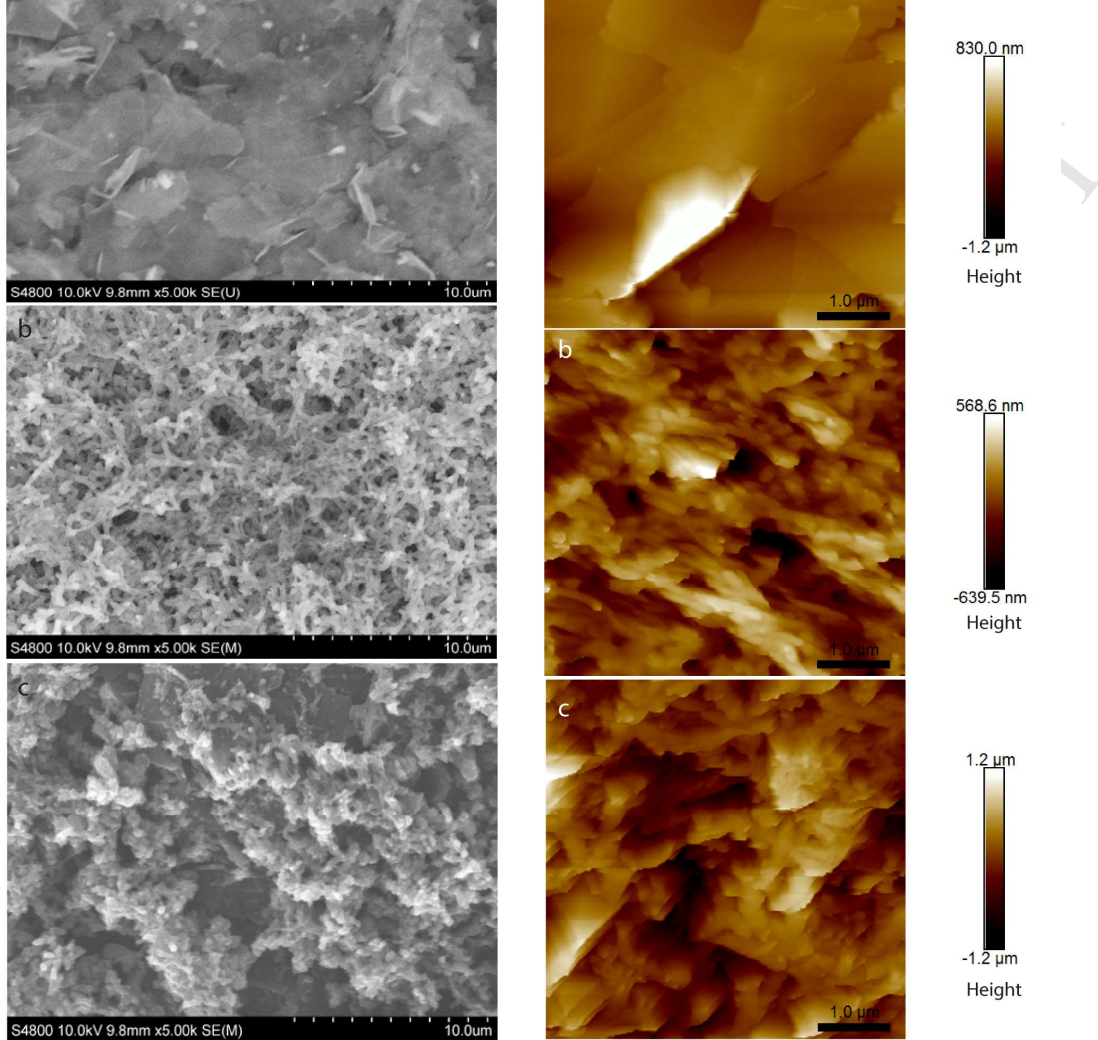
369 The combined detection of two different epigenetic marks, using a unified detection platform, now opens
370 the way to monitoring multiple epigenetic modifications, particularly targeting the multitude of
371 modifications that occur on histone proteins, which as well as acetylation, include protein methylation,
372 ubiquitylation, phosphorylation, sumoylation, ribosylation and citrullination. Developments in smaller,
373 multiplexed sensors are now required, and could result in a move from SPEs to emerging FET-based
374 systems (Campos et al., 2019).

375 **Acknowledgments**

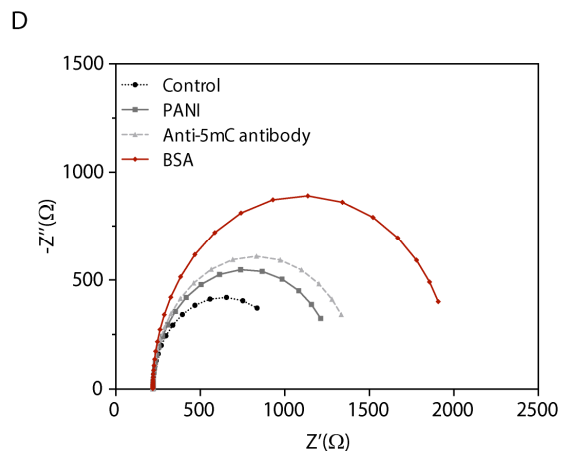
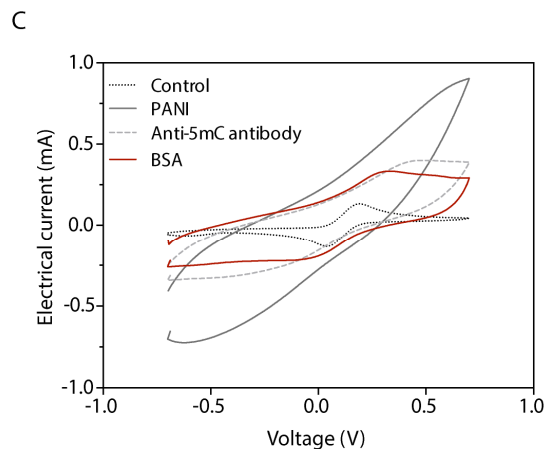
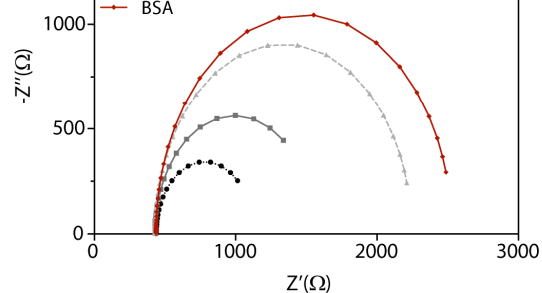
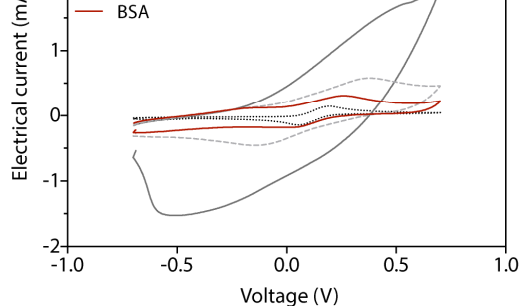
376 **Funding:** S.T. Welsh National Research Network in Advanced Engineering and Materials (NRNF77).
377 I.M.P. Marie Curie COFUND Programme “NanoTRAINforGrowth” from the European Union’s Seventh
378 Framework Programme for research, technological development and demonstration under grant agreement
379 no 600375. This article is a result of the project Advancing cancer research: from basic knowledge to
380 application (NORTE-01-0145-FEDER-000029), co-financed by Norte Portugal Regional Operational
381 Programme (NORTE 2020), under the PORTUGAL 2020 Partnership Agreement, through the European
382 Regional Development Fund (ERDF).

383 **Author contributions:** S.R.T. study design, sensor design, fabrication and data collection. L.P. and J.D.
384 ChIP and MeDIP and data analysis. C.M.A. data analysis, figure and manuscript preparation. S.Y. and
385 A.S. sensor fabrication, data collection, data analysis. L.M. expert clinical input in manuscript preparation.
386 I.M.P. sensor design and fabrication, data analysis, manuscript preparation. D.G. study design, manuscript
387 preparation. L.W.F. study concept and design, manuscript preparation. R.S.C. study concept and design,
388 manuscript preparation.

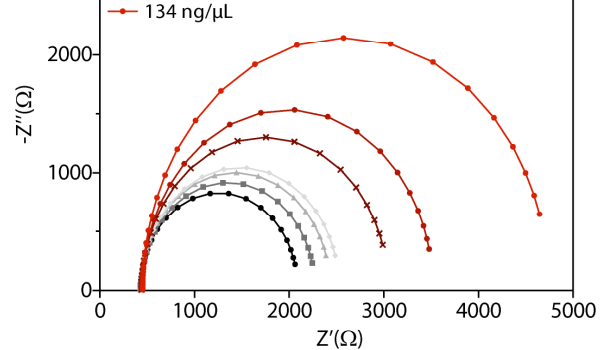
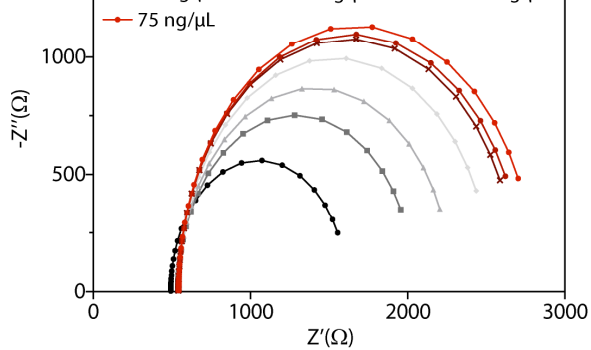
389 **Competing interests:** The authors declare that they have no competing interests.
390
391



393
 394 **Fig. S1. Surface characterization of biosensor assembly.** (A) Scanning Electron Microscopy of (a) unmodified
 395 graphene; (b) graphene modified with PANI (C); anti-ach3 attached to the PANI layer; (B) Atomic Force
 396 Microscopy of (a) unmodified graphene; (b) graphene modified with PANI (c); anti-ach3 attached to the PANI layer.

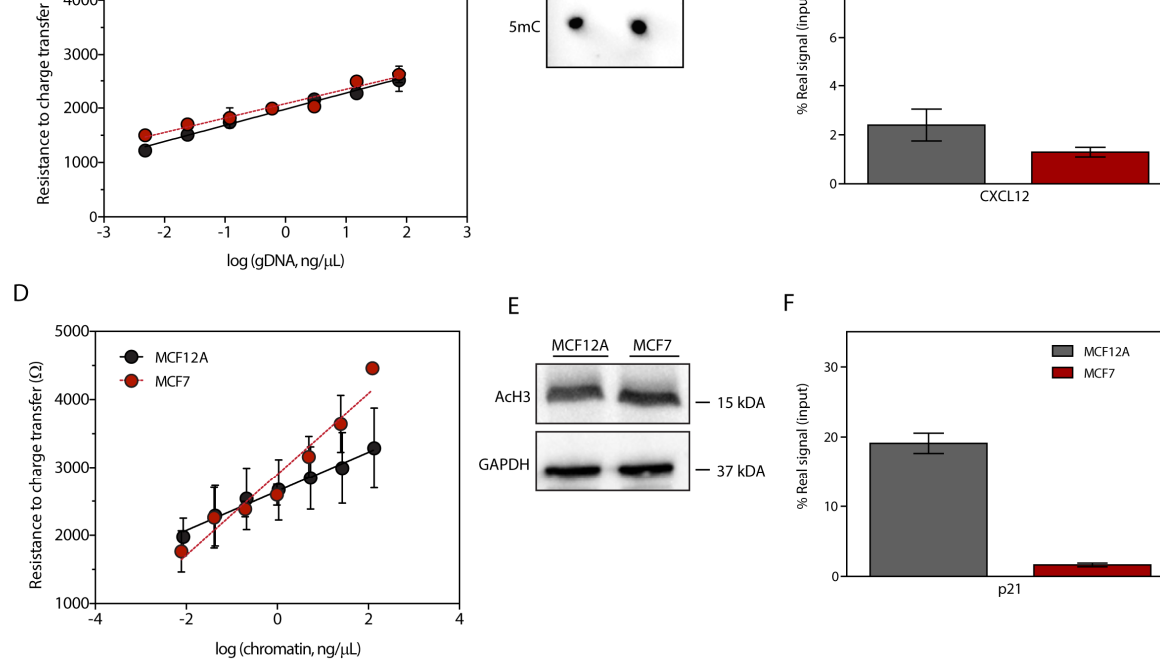


397
398 **Fig 1. Electrochemical characterization of biosensor assembly.** (A) Cyclic voltammogram (CV) of the acetylation
399 immunosensor assembly after each modification of graphene-SPE/PANI/anti-acH3/BSA. (B) Nyquist plots of
400 graphene-SPE/PANI/anti-acH3/BSA sensor, obtained in 5.0mM $[\text{Fe}(\text{CN})_6]^{3-/4-}$ PBS buffer pH 7.4. (C) CV of the
401 methylation immunosensor assembly after each modification of graphene-SPE/PANI/anti-5mC/BSA (D) Nyquist
402 plots of graphene-SPE/PANI/anti-5mC/BSA sensor, obtained in 5.0mM $[\text{Fe}(\text{CN})_6]^{3-/4-}$ PBS buffer pH 7.4.
403



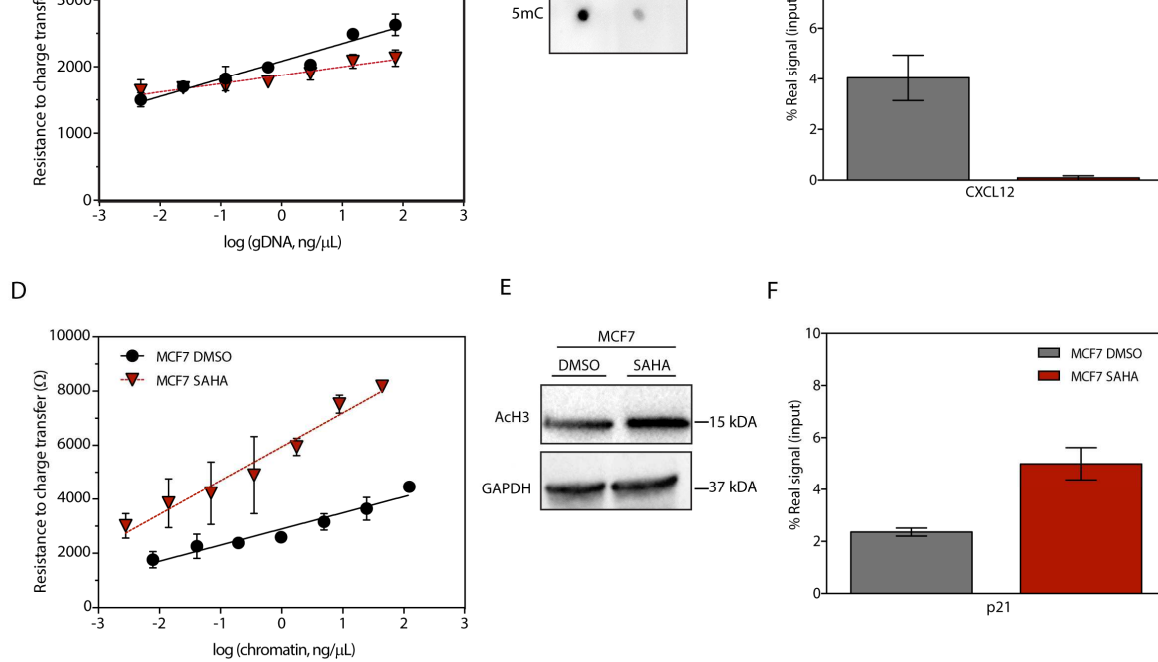
404
 405 **Fig. 2. Global epigenetic modifications in breast cells (MCF12A).** (A) Representative Nyquist plot of the
 406 methylation biosensor upon detection of increasing concentrations of gDNA (B) Representative Nyquist plot of the
 407 acetylation biosensor upon detection of increasing concentrations of chromatin.

ACCEPTED MANUSCRIPT



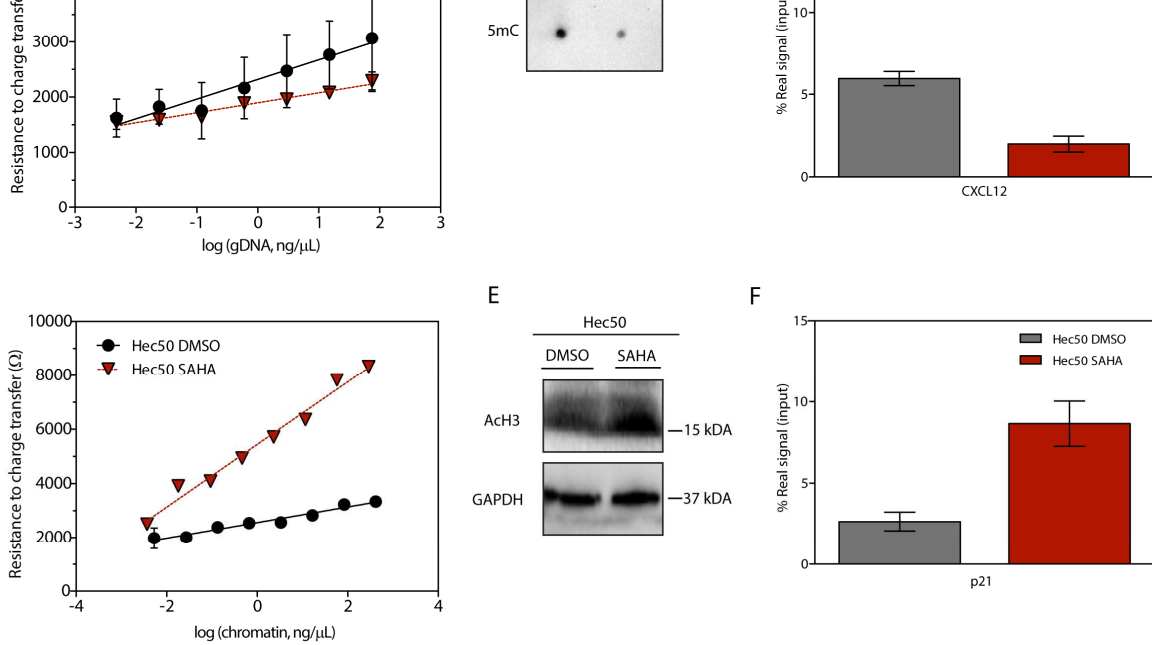
408
409

Fig. 3. Detection of global (A, B, D and E) and locus (C and F) modifications in breast cancer cells. (A) Calibration curve, plotting log(gDNA) against Rct for MCF12A and MCF7. Error bars represent the standard error of the mean of three biological replicates. (B) Dot blotting of global methylation for MCF12A versus MCF7 using gDNA with anti-5mC antibody. (C) MeDIP enrichment of CXCL12 from 500 ng MCF12A and MCF7 gDNA by MeDIP using anti-5mC antibody relative to a non-specific IgG reported as % real signal (% positive antibody - % IgG, relative to a standard gDNA input sample). Error bars represent the standard error of the mean of three biological replicates. (D) Calibration curve, plotting log(chromatin) against Rct for MCF12A and MCF7. Error bars represent the standard error of the mean of three biological replicates. (E) Western blot detection of global acetylated histone H3 (acH3) in MCF12A and MCF7 chromatin using a specific antibody directed against the modified histone protein. (F) Enrichment of the human p21 locus associated with acetylated histone H3 by ChIP using 1 μg MCF12A and MCF7 chromatin. Error bars represent the standard error of the mean of three biological replicates.



421

422 **Fig. 4. Detection of global (A, B, D and E) and locus (C and F) modifications in breast cancer cells (MCF7)**
 423 **upon treatment.** (A) Calibration curve, plotting log(gDNA) against Rct for MCF7 treated versus MCF7 untreated.
 424 Error bars represent the standard error of the mean of three biological replicates. (B) Dot blotting of global
 425 methylation for MCF7 treated versus untreated using gDNA with anti-5mC antibody. (C) MeDIP enrichment of
 426 CXCL12 from 500 ng MCF7 treated and MCF7 untreated gDNA using anti-5mC antibody relative to a non-specific
 427 IgG. Error bars represent the standard error of the mean of three biological replicates. (D) Calibration curve, plotting
 428 log(chromatin) against Rct for MCF7 treated versus MCF7 untreated. Error bars represent the standard error of the
 429 mean of three biological replicates. (E) Western blot detection of global acetylated histone 3 (acH3) in MCF7 treated
 430 versus untreated chromatin using a specific antibody directed against the modified histone protein. (F) Enrichment of
 431 the human p21 locus associated with acetylated histone H3 by ChIP using 1 μg MCF7 treated and MCF7 untreated
 432 chromatin. Error bars represent the standard error of the mean of three biological replicates.
 433



434

435 **Fig. 5. Detection of global (A, B, D and E) and locus (C and F) modifications in endometrial cells (Hec50) upon**
 436 **treatment. (A)** Calibration curve, plotting log(gDNA) against Rct for Hec50 treated versus Hec50 untreated. Error
 437 bars represent the standard error of the mean of three biological replicates. **(B)** Dot blotting of global methylation for
 438 Hec50 treated versus Hec50 untreated using gDNA with anti-5mC antibody. **(C)** MedIP enrichment of CXCL12
 439 from 500 ng Hec50 treated and untreated gDNA by MedIP using anti-5mC antibody relative to a non-specific IgG
 440 demonstrates. Error bars represent the standard error of the mean of three biological replicates. **(D)** Calibration curve,
 441 plotting log(chromatin) against Rct for Hec50 treated versus Hec50 untreated. Error bars represent the standard error
 442 of the mean of three biological replicates. **(E)** Western blot detection of global acetylated histone 3 (acH3) in Hec50
 443 treated versus Hec50 untreated chromatin using a specific antibody directed against the modified histone protein. **(F)**
 444 Enrichment of the human p21 locus associated with acetylated histone H3 by ChIP using 1 µg Hec50 treated
 445 untreated chromatin. Error bars represent the standard error of the mean of three biological replicates.

446

447

- 452 Arik, D., Dooner, R., Dasato, F., Campai, M., Dam, C., Danneke, C.M., Diep, D., Fernandez, A.F.,
453 Gerhauser, C., Haake, A., Heilmann, K., Holcomb, T., Hussmann, D., Ito, M., Kläver, R., Kreutz, M.,
454 Kulis, M., Lopez, V., Nair, S.S., Paul, D.S., Plongthongkum, N., Qu, W., Queirós, A.C., Reinicke, F.,
455 Sauter, G., Schlomm, T., Statham, A., Stirzaker, C., Strogantsev, R., Urduingio, R.G., Walter, K.,
456 Weichenhan, D., Weisenberger, D.J., Beck, S., Clark, S.J., Esteller, M., Ferguson-Smith, A.C., Fraga,
457 M.F., Guldberg, P., Hansen, L.L., Laird, P.W., Martín-Subero, J.I., Nygren, A.O.H., Peist, R., Plass,
458 C., Shames, D.S., Siebert, R., Sun, X., Tost, J., Walter, J., Zhang, K., 2016. Quantitative comparison
459 of DNA methylation assays for biomarker development and clinical applications. *Nat. Biotechnol.*
<https://doi.org/10.1038/nbt.3605>
- 460 Bormann, F., Rodríguez-Paredes, M., Lasitschka, F., Edelman, D., Musch, T., Benner, A., Bergman, Y.,
461 Dieter, S.M., Ball, C.R., Glimm, H., Linhart, H.G., Lyko, F., 2018. Cell-of-Origin DNA Methylation
462 Signatures Are Maintained during Colorectal Carcinogenesis. *Cell Rep.*
463 <https://doi.org/10.1016/j.celrep.2018.05.045>
- 464 Butler, J.S., Dent, S.Y.R., 2013. The role of chromatin modifiers in normal and malignant hematopoiesis.
465 *Blood.* <https://doi.org/10.1182/blood-2012-10-451237>
- 466 Campos, R., Borme, J., Guerreiro, J.R., Machado, G., Cerqueira, M.F., Petrovykh, D.Y., Alpuim, P., 2019.
467 Attomolar label-free detection of dna hybridization with electrolyte-gated graphene field-effect
468 transistors. *ACS Sensors* 4, 286–293. <https://doi.org/10.1021/acssensors.8b00344>
- 469 Capp, J.P., 2017. Tissue disruption increases stochastic gene expression thus producing tumors: Cancer
470 initiation without driver mutation. *Int. J. Cancer.* <https://doi.org/10.1002/ijc.30596>
- 471 Coleman, N., De, S., 2018. Mutation Signatures Depend on Epigenomic Contexts. *Trends Cancer* 4, 659–
472 661.
- 473 Daniels, J.S., Pourmand, N., 2007. Label-free impedance biosensors: Opportunities and challenges.
474 *Electroanalysis.* <https://doi.org/10.1002/elan.200603855>
- 475 Dawson, M.A., Kouzarides, T., 2012. Cancer Epigenetics: From Mechanism to Therapy. *Cell* 150, 12–27.
- 476 Flavahan, W.A., Gaskell, E., Bernstein, B.E., 2017. Epigenetic plasticity and the hallmarks of cancer.
477 *Science* (80-.). <https://doi.org/10.1126/science.aal2380>
- 478 Gazze, A., Ademefun, R., Conlan, R.S., Teixeira, S.R., 2018. Electrochemical impedance spectroscopy
479 enabled CA125 detection; toward early ovarian cancer diagnosis using graphene biosensors. *J.*
480 *Interdiscip. Nanomedicine* 3, 82–88. <https://doi.org/10.1002/jin2.40>
- 481 Graff-Baker, A.N., Orozco, J.I.J., Marzese, D.M., Salomon, M.P., Hoon, D.S.B., Goldfarb, M., 2018.
482 Epigenomic and Transcriptomic Characterization of Secondary Breast Cancers. *Ann. Surg. Oncol.*
483 <https://doi.org/10.1245/s10434-018-6582-7>
- 484 Guo, F., Wang, Y., Liu, J., Mok, S.C., Xue, F., Zhang, W., 2016. CXCL12/CXCR4: A symbiotic bridge
485 linking cancer cells and their stromal neighbors in oncogenic communication networks. *Oncogene.*
486 <https://doi.org/10.1038/onc.2015.139>
- 487 Hall, R.H., 1971. *The modified nucleosides in nucleic acids.* Columbia University Press (1971).
- 488 Jones, P.A., Baylin, S.B., 2007. The Epigenomics of Cancer. *Cell* 128, 683–692.
- 489 Koo, K.M., Sina, A.A.I., Carrascosa, L.G., Shiddiky, M.J.A., Trau, M., 2015. DNA-bare gold affinity
490 interactions: Mechanism and applications in biosensing. *Anal. Methods.*
491 <https://doi.org/10.1039/c5ay01479d>
- 492 Krejcova, L., Richtera, L., Hynek, D., Labuda, J., Adam, V., 2017. Current trends in electrochemical
493 sensing and biosensing of DNA methylation. *Biosens. Bioelectron.* 97, 384–399.
494 <https://doi.org/10.1016/J.BIOS.2017.06.004>

- 499 Lo, P.K., Zhou, Q., 2018. Emerging Techniques in Single-Cell Epigenomics and their Applications to
500 Cancer Research. *J. Clin. Genomics* 1, 1–8.
- 501 Luu, T., Kim, K. pyo, Blanchard, S., Anyang, B., Hurria, A., Yang, L., Beumer, J.H., Somlo, G., Yen, Y.,
502 2018. Phase IB trial of ixabepilone and vorinostat in metastatic breast cancer. *Breast Cancer Res.*
503 *Treat.* 167, 469–478. <https://doi.org/10.1007/s10549-017-4516-x>
- 504 Mossman, D., Kim, K.T., Scott, R.J., 2010. Demethylation by 5-aza-2'-deoxycytidine in colorectal cancer
505 cells targets genomic DNA whilst promoter CpG island methylation persists. *BMC Cancer.*
506 <https://doi.org/10.1186/1471-2407-10-366>
- 507 Qu, K., Zaba, L.C., Satpathy, A.T., Giresi, P.G., Li, R., Jin, Y., Armstrong, R., Jin, C., Schmitt, N.,
508 Rahbar, Z., Ueno, H., Greenleaf, W.J., Kim, Y.H., Chang, H.Y., 2017. Chromatin Accessibility
509 Landscape of Cutaneous T Cell Lymphoma and Dynamic Response to HDAC Inhibitors. *Cancer*
510 *Cell.* <https://doi.org/10.1016/j.ccell.2017.05.008>
- 511 Ramos, M.P., Wijetunga, N.A., McLellan, A.S., Suzuki, M., Grealley, J.M., 2015. DNA demethylation by
512 5-aza-2'-deoxycytidine is imprinted, targeted to euchromatin, and has limited transcriptional
513 consequences. *Epigenetics and Chromatin.* <https://doi.org/10.1186/s13072-015-0004-x>
- 514 Rendeiro, A.F., Schmidl, C., Strefford, J.C., Walewska, R., Davis, Z., Farlik, M., Oscier, D., Bock, C.,
515 2016. Chromatin accessibility maps of chronic lymphocytic leukaemia identify subtype-specific
516 epigenome signatures and transcription regulatory networks. *Nat. Commun.*
517 <https://doi.org/10.1038/ncomms11938>
- 518 Roh, T.Y., Cuddapah, S., Zhao, K., 2005. Active chromatin domains are defined by acetylation islands
519 revealed by genome-wide mapping. *Genes Dev.* <https://doi.org/10.1101/gad.1272505>
- 520 Sánchez, S., Roldán, M., Pérez, S., Fàbregas, E., 2008. Toward a fast, easy, and versatile immobilization
521 of biomolecules into carbon nanotube/polysulfone-based biosensors for the detection of hCG
522 hormone. *Anal. Chem.* <https://doi.org/10.1021/ac7025282>
- 523 Sawhney, M., Conlan, R., 2019. POISED-5, a Portable On-board Electrochemical Impedance
524 Spectroscopy Biomarker Analysis Device. *Biomed Microdevices.*
525 <https://doi.org/https://doi.org/10.1007/s10544-019-0406-9>
- 526 Sheahan, A. V, Ellis, L., 2018. Epigenetic reprogramming: A key mechanism driving therapeutic
527 resistance. *Urol Oncol* 36, 375–379.
- 528 Singh, A.A., Petraglia, F., Nebbioso, A., Yi, G., Conte, M., Valente, S., Mandoli, A., Scisciola, L.,
529 Lindeboom, R., Kerstens, H., Janssen-Megens, E.M., Pourfarzad, F., Habibi, E., Berentsen, K., Kim,
530 B., Logie, C., Heath, S., Wierenga, A.T.J., Clarke, L., Flicek, P., Jansen, J.H., Kuijpers, T., Yaspo,
531 M.L., Della Valle, V., Bernard, O., Gut, I., Vellenga, E., Stunnenberg, H.G., Mai, A., Altucci, L.,
532 Martens, J.H.A., 2018. Multi-omics profiling reveals a distinctive epigenome signature for high-risk
533 acute promyelocytic leukemia. *Oncotarget.* <https://doi.org/10.18632/oncotarget.25429>
- 534 Stewart, C.M., Tsui, D.W.Y., 2018. Circulating cell-free DNA for non-invasive cancer management.
535 *Cancer Genet.* <https://doi.org/10.1016/j.cancergen.2018.02.005>
- 536 Teixeira, S., Conlan, R.S., Guy, O.J., Sales, M.G.F., 2014a. Label-free human chorionic gonadotropin
537 detection at picogram levels using oriented antibodies bound to graphene screen-printed electrodes. *J.*
538 *Mater. Chem. B* 2, 1852–1865. <https://doi.org/10.1039/c3tb21235a>
- 539 Teixeira, S., Conlan, R.S., Guy, O.J., Sales, M.G.F., 2014b. Label-free human chorionic gonadotropin
540 detection at picogram levels using oriented antibodies bound to graphene screen-printed electrodes. *J.*
541 *Mater. Chem. B* 2, 1852. <https://doi.org/10.1039/c3tb21235a>
- 542 Teixeira, S.R., Lloyd, C., Yao, S., Andrea Salvatore Gazze, Whitaker, I.S., Francis, L., Conlan, R.S.,

546 fluorometric biosensor for label-free and homogenous detection of protein acetylation-related
547 enzymes activities. *Biosens. Bioelectron.* 91, 400–407. <https://doi.org/10.1016/j.bios.2016.12.065>

548 Xi, Y., Shi, J., Li, Wenqian, Tanaka, K., Allton, K.L., Richardson, D., Li, J., Franco, H.L., Nagari, A.,
549 Malladi, V.S., Coletta, L. Della, Simper, M.S., Keyomarsi, K., Shen, J., Bedford, M.T., Shi, X.,
550 Barton, M.C., Lee Kraus, W., Li, Wei, Dent, S.Y.R., 2018. Histone modification profiling in breast
551 cancer cell lines highlights commonalities and differences among subtypes. *BMC Genomics*.
552 <https://doi.org/10.1186/s12864-018-4533-0>

553 Zhang, J., Han, X., Gao, C., Xing, Y., Qi, Z., Liu, R., Wang, Y., Zhang, X., Yang, Y.G., Li, X., Sun, B.,
554 Tian, X., 2018. 5-Hydroxymethylome in Circulating Cell-free DNA as A Potential Biomarker for
555 Non-small-cell Lung Cancer. *Genomics, Proteomics Bioinforma.*
556 <https://doi.org/10.1016/j.gpb.2018.06.002>

557 Zhu, C., Yang, G., Li, H., Du, D., Lin, Y., 2015. Electrochemical sensors and biosensors based on
558 nanomaterials and nanostructures. *Anal. Chem.* <https://doi.org/10.1021/ac5039863>

559 Zor, E., Hatay Patir, I., Bingol, H., Ersoz, M., 2013. An electrochemical biosensor based on human serum
560 albumin/graphene oxide/3-aminopropyltriethoxysilane modified ITO electrode for the
561 enantioselective discrimination of d- and l-tryptophan. *Biosens. Bioelectron.*
562 <https://doi.org/10.1016/j.bios.2012.10.068>

563

methylation and histone H3 acetylation levels. The system application demonstrated global alterations in DNA methylation or histone H3 acetylation in response to treatment with decitabine and vorinostat respectively.

- System application demonstrated global alterations in DNA methylation or histone H3 acetylation in response to treatment with decitabine and vorinostat respectively.
- Results were corroborated using established techniques including ChIP and MeDIP.
- The study opens up the opportunity for assessing point-of-care monitoring of patient responses to epigenetic therapeutics, and multiplexing epigenetic marker detection on a unified platform.

ACCEPTED MANUSCRIPT

J.D. Resources; Formal analysis

C.M.A. Validation; Writing - original draft; Writing - review & editing

S.Y. Resources; Software; Validation

A.S. Resources; Software; Validation

L.M. Conceptualization; Writing - review & editing

I.M.P. Conceptualization; Investigation; Supervision; Validation; Visualization; Writing - original draft; Writing - review & editing

D.G. Conceptualization; Supervision; Writing - original draft; Writing - review & editing

L.W.F. Conceptualization; Writing - original draft; Writing - review & editing

R.S.C. Conceptualization; Funding acquisition; Supervision; Writing - original draft; Writing - review & editing

ACCEPTED MANUSCRIPT